The days of plenty might soon be over in glacierized Central Asian catchments

Supplementary Information

Annina Sorg*[1,2], Matthias Huss[3] Mario Rohrer[4] and Markus Stoffel[1,2]

[1] Institute for Environmental Sciences (ISE), University of Geneva, Route de Drize 7, 1227 Carouge, Switzerland

[2] dendrolab.ch, Institute of Geological Sciences, University of Berne, Baltzerstrasse 1+3, 3000 Bern, Switzerland

[3] Department of Geosciences, University of Fribourg, 1700 Fribourg, Switzerland

[4] Meteodat GmbH, Technoparkstrasse 1, 8005 Zurich, Switzerland

1. Data

We used exceptionally long data series of temperature, precipitation, discharge and glacier mass balance to run and calibrate a distributed glacio-hydrological runoff model (Fig. S1).

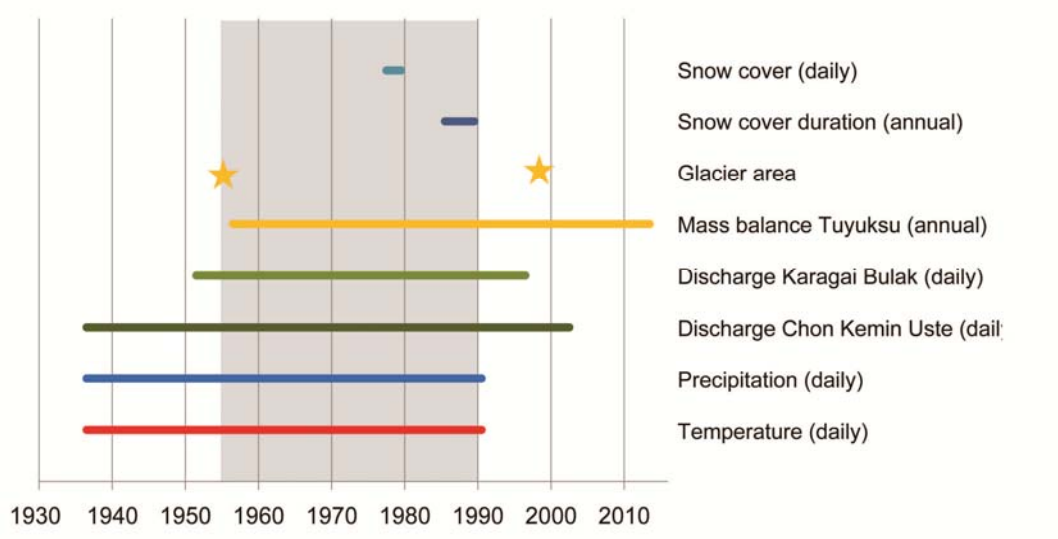

Fig. S1. Data coverage for model input and calibration, with calibration period (1955-1989) displayed in grey.

Temperature and **precipitation** time series from Sabdan station (42.70°N, 76.10°E, 1524 m asl, WMO N° 36921) were available in daily resolution for the time period 1937-1990. The data were downloaded from the Royal Netherlands Meteorological Institute (KNMI) Climate Explorer (http://climexp.knmi.nl).
The precipitation data series contained gaps (02/1955, 1966-1976, 10/1977, 04/1985, 06/1986, 04/07/12/1987), which we filled with daily data from the National Climatic Data Center NOAA (http://www1.ncdc.noaa.gov/pub/data/documentlibrary/tddoc/td9290c.pdf). As the quality of the NOAA data is likely to be lower than the quality of the KNMI data, we have excluded the period 1966-1976 for detailed calibration and used it only to approximate the transient glacier evolution in the past.
As the year 1999 marks the turning point between “past” and “future” in our model, we have extended the measured temperature and precipitation series with downscaled data from the most moderate scenario (dry-cold scenario, see Chapter 4 below) for the period 1990-1999 to allow continuous modeling from 1955 to 2099. The period 1990-1999 is, like 1966-1976, not analyzed in detail.

Discharge data for Chon Kemin Uste (42.67°N, 75.91°E, 1289 m asl) and Karagai Bulak (42.80°N, 76.41°E, 2078 m asl) gauges were available in daily resolution for the time periods 1936-2002 and 1951-1996, respectively. The data were provided by the Kyrgyz National Hydrometeorological Agency (Kirgizgidromet, 1936-2002) and digitized by the authors of this study.

Mass balance and **equilibrium line altitude (ELA)** have been assessed since 1957 at Tuyuksu glacier, which makes them the longest series in Central Asia. We have received the data from the (WGMS Haeberli *et al.*, 2009), the original author is P. A. Cherkasov.

Glacier outlines are from (Bolch, 2007), who mapped the glacier coverage in the Chon Kemin and surrounding valleys using a snow-free Landsat ETM+ scene from 08/08/1999. A TM4/TM5 ratio image was used to delineate the glaciers and misclassified pixels of vegetated areas and lakes were eliminated using the Normalized Difference Vegetation Index (NDVI). We have also digitized glacier outlines reflecting the situation in the 1950s based on topographic maps (Soviet Topographic Map, 1988) to calibrate the model.

Landuse classification for the three non-glacier surface types classified in GERM (forest, vegetation and bare surfaces) has been derived from a supervised classification in Erdas Imagine 8.4 of the same Landsat ETM+ scene as used for the glacier outlines.

Daily snow cover has been used for visual comparison from four Landsat scenes in 1977 (17/04, 23/05, 07/09 and 01/11) and two Landsat scenes in 1979 (30/03 and 12/05). All Landsat scenes were downloaded from http://earthexplorer.usgs.gov/.

Annual snow cover duration has been assessed from the Advanced Very High Resolution Radiometer (AVHRR) at a resolution of 1 km starting in 1986 (Dietz *et al.*, 2013). The data were provided by Andreas Dietz.

The digital elevation model (DEM) and **catchment area delineation** are based on data from the Shuttle Radar Topography Mission SRTM3 (Jarvis *et al.*, 2008). The DEM was resampled from 90 meters to the model resolution of 200 meters. From the SRTM3 DEM, the catchment outline has been derived with ArcGIS Hydrotools. SRTM data were downloaded from http://srtm.csi.cgiar.org/SELECTION/inputCoord.asp.

2. Statistical trend analysis (Mann-Kendall trend test)

Trends in temperature, precipitation and runoff were analyzed with the 2-sided non-parametric Mann-Kendall trend test at the 80, 90 and 95% significance levels (Kendall, 1975; Helsel and Hirsch, 1992). Serial correlation was removed using Sen's slope method (Sen, 1968) and Xuebin Zhang's pre-whitening approach (Zhang *et al.*, 2000). With the help of moving time windows, the multiple trend tests were computed for all time windows of at least 30 years in length during the common 1937-1990 period. The trend matrices in Fig. S2 show the resulting trends (standardized test statistic Z_{MK}; tau) and significance levels (2-sided *p*-value) for key climate variables.

Next 2 pages:
Fig. S2. Summary of the Mann-Kendall (MK) trend test statistics. Trend significance is indicated by the 2-sided p-value and trends are indicated with the standardized test statistics tau.

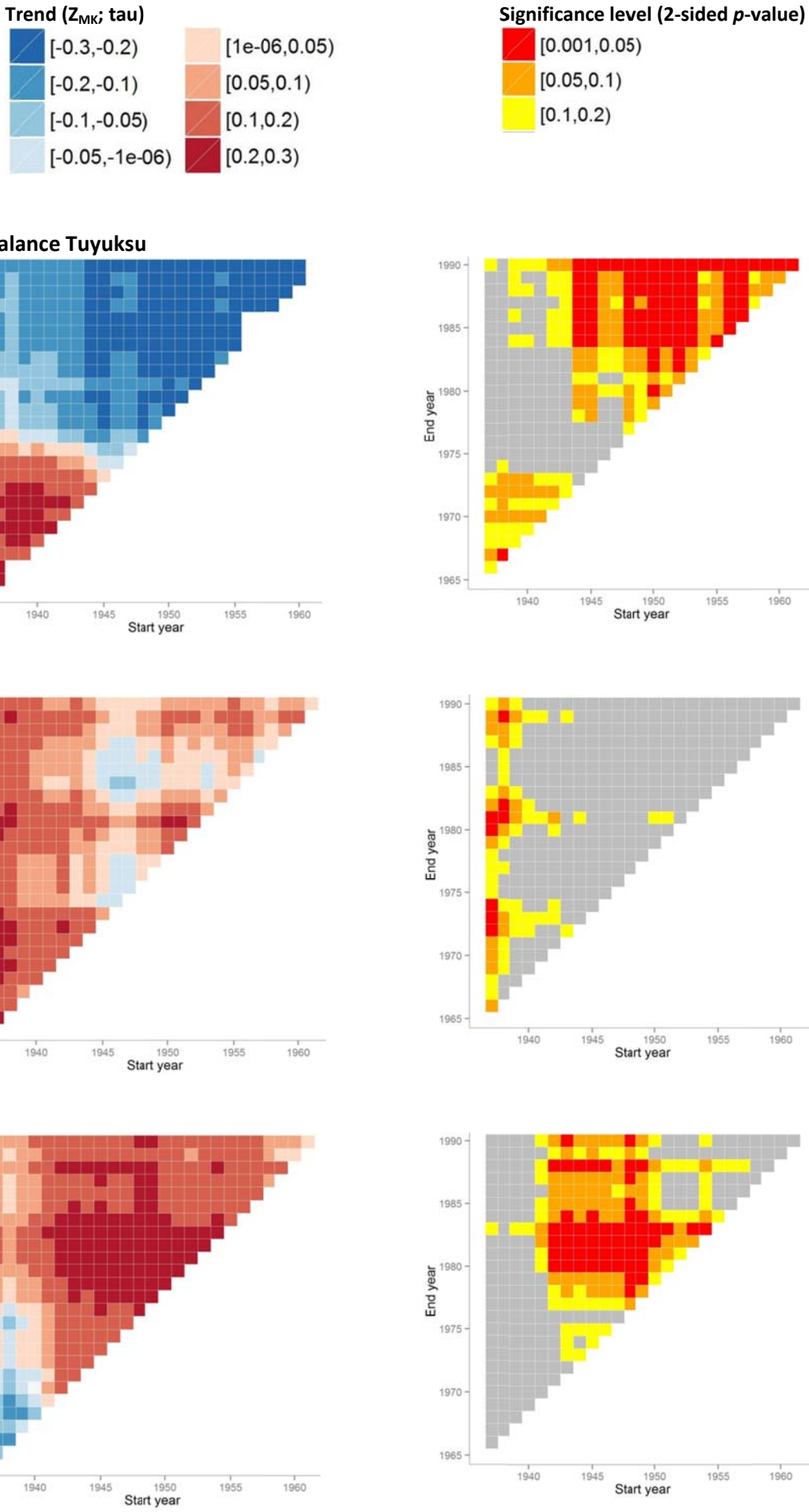
Trend (Z_{MK}; tau)
[-0.3,-0.2)
[-0.2,-0.1)
[-0.1,-0.05)
[-0.05,-1e-06)
[1e-06,0.05)
[0.05,0.1)
[0.1,0.2)
[0.2,0.3)
Significance level (2-sided p-value)
[0.001,0.05)
[0.05,0.1)
[0.1,0.2)
Mass balance Tuyuksu
MAP
MAAT
End year
Start year
1990
1985
1980
1975
1970
1965
1940
1945
1950
1955
1960

Summer temperature (JJA)

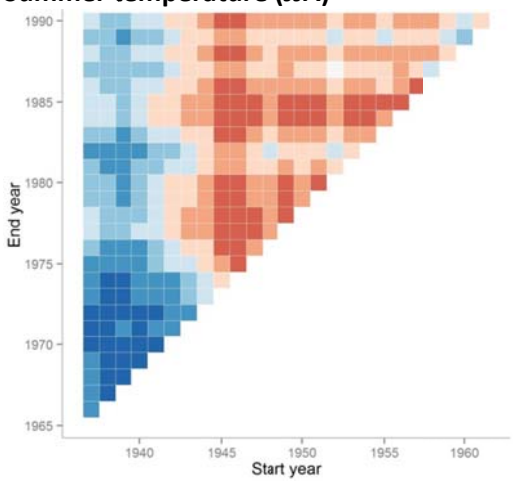

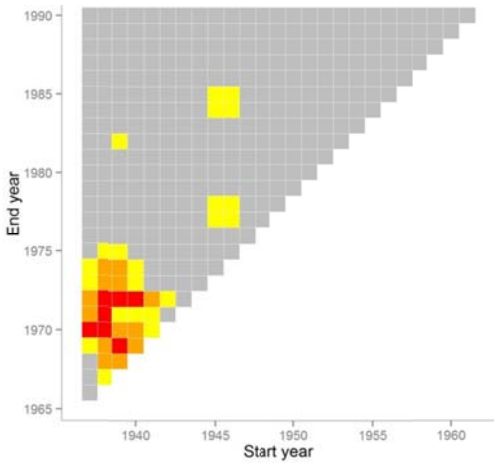

Total runoff Uste

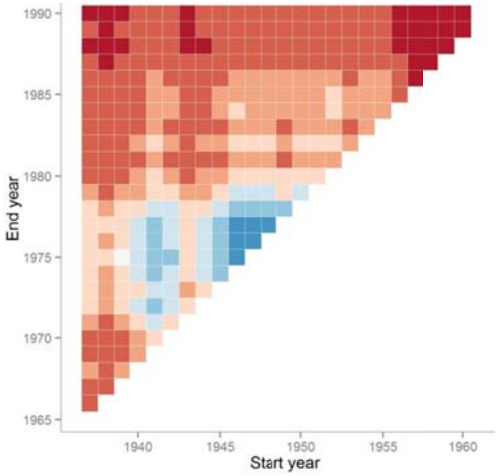

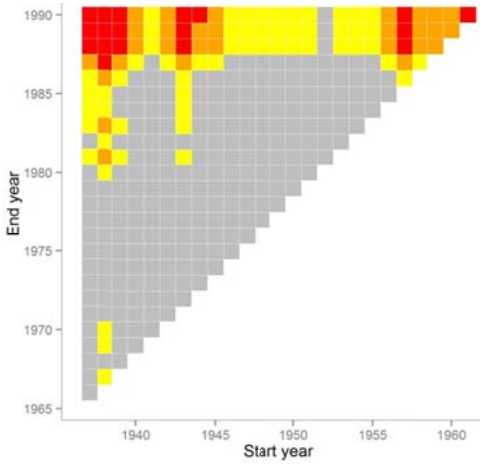

Summer runoff Uste (JJA)

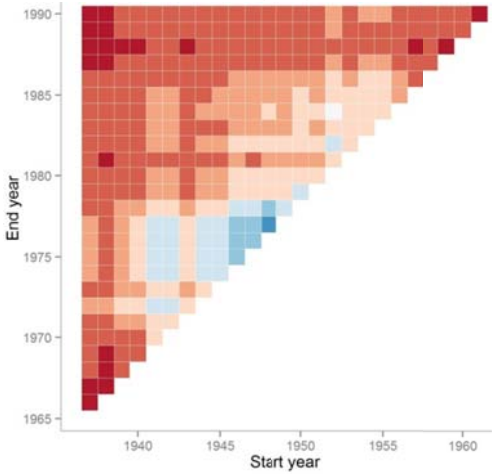

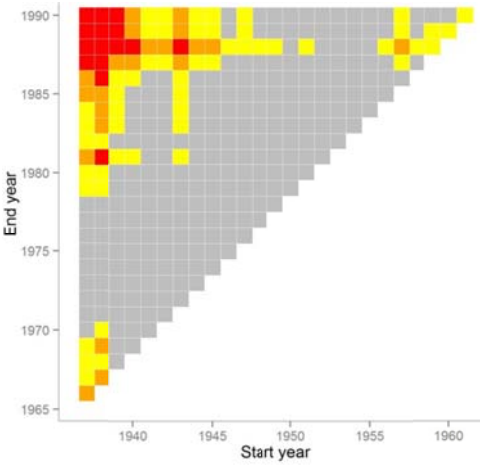

3. Climate data generation

We evaluated all available Global Circulation Model (GCM) runs for the two most extreme representative concentration pathways scenarios (Meinshausen *et al.*, 2011), RCPs 2.6 and 8.5, generated under the Climate Model Intercomparison Project CMIP5 (Taylor *et al.*, 2012) to cover the whole range of possible climatic changes (Vuuren *et al.*, 2011). Under the RCP 2.6 scenario, greenhouse gas emissions and emissions of air pollutants are reduced substantially over time. RCP 8.5 is characterized by increasing greenhouse gas emissions over time representative of scenarios leading to high greenhouse gas concentration levels. All GCM data were downloaded from http://cmip-pcmdi.llnl.gov/cmip5 (01/09/2013).

Downscaling of large-scale GCM output to a finer spatial resolution can be done either with dynamical or statistical approaches (Fowler *et al.*, 2007). Whereas dynamical downscaling requires a higher resolution regional climate model (RCM) to be embedded within a GCM, statistical downscaling establishes empirical relationships between GCM-resolution climate variables and local climate.

We used the statistical "perturbation method" or "delta-change approach" (Prudhomme *et al.*, 2002; Huss *et al.*, 2008b; Smith and Pitts, 1997), thus applying differences between the control and future GCM simulations to baseline observations by adding (temperature) or scaling (precipitation) the mean climatic change to each day. Following the method described in Huss *et al.* (2008b), we use the daily variability of measured time series at Sabdan station and adapt their monthly means along the linear trend line between the standard WMO baseline period (1961-1990) and our future reference period (2081-2099). Using this technique, we obtain meteorological time series with the same resolution, characteristics and variance as in the past.

We then compared all RCP 2.6 and 8.5 GCM runs regarding changes in summer temperature and annual precipitation (mean 2081-2099 vs. 1961-1990; Fig. S3) and chose the four GCM runs which are closest to the 10^{th} and 90^{th} percentiles (Fig. S3), thus representing the range of dry-cold, dry-warm, wet-cold and wet-warm future climates (Immerzeel *et al.*, 2013; Lutz *et al.*, 2013).

Next page:
Fig. S3. Projected changes in climate at Sabdan station, Chon Kemin valley, according to RCPs 2.6 and 8.5 of the CMIP5 dataset. **a**, Changes in summer temperature and annual precipitation based on all GCM runs for 75-77.5°E and 40-45°N (baseline period 1961-1990 vs future period 2081-2099). The range between the 10^{th} and 90^{th} percentiles is shaded in grey. The four GCM runs closest to the percentiles have been chosen for runoff modeling. **b** and **c**, Time series of annual precipitation and summer temperature anomalies for Sabdan meteorological station relative to the 1961-1990 baseline period. The four scenarios represent the range of dry-cold, dry-warm, wet-cold and wet-warm future climates as displayed in Fig. 3a.

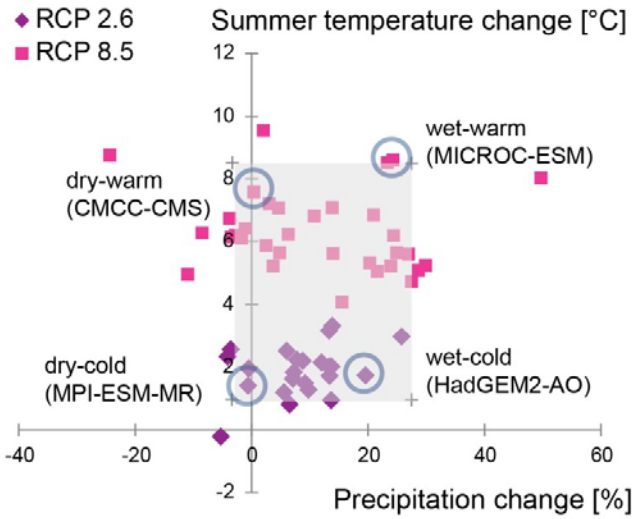
RCP 2.6
RCP 8.5
Summer temperature change [°C]
12
10
8
6
4
2
-2
wet-warm
(MICROC-ESM)
dry-warm
(CMCC-CMS)
dry-cold
(MPI-ESM-MR)
wet-cold
(HadGEM2-AO)
-40
-20
0
20
40
60
Precipitation change [%]

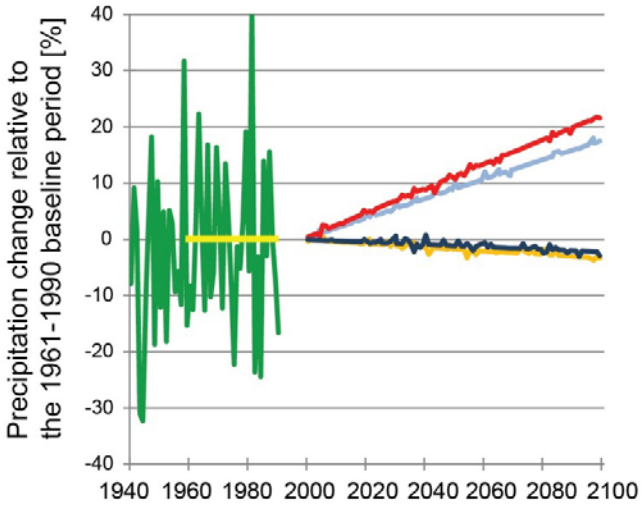
Precipitation change relative to the 1961-1990 baseline period [%]
40
30
20
10
0
-10
-20
-30
-40
1940
1960
1980
2000
2020
2040
2060
2080
2100

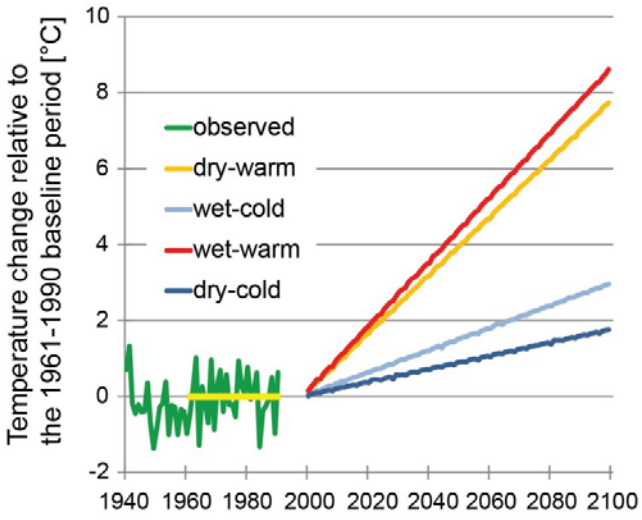
Temperature change relative to the 1961-1990 baseline period [°C]
10
8
6
4
2
0
-2
observed
dry-warm
wet-cold
wet-warm
dry-cold
1940
1960
1980
2000
2020
2040
2060
2080
2100

4. Glacier Evolution Runoff Model GERM

4.1 Calibration and validation procedure

Table S1. Multi-variable calibration of GERM developed for this study.

Parameter group	Criteria	Selection
Climate	Precipitation (4000 m asl)	values from Aizen et al. 2007 ± 10%
	Mean annual evaporation	
	Mean annual runoff	observed ± 10%
Melt	Daily snow cover	visual
	Annual snow cover	observed ± 10%
	Mass balance and ELA	
	Glacier area change	
Routing	Monthly runoff	NS > 0.8

Table S2. Key model parameters of GERM.

Description	Parameter	Value	Unit	Source / Calibrated
Climate parameters				
Precipitation gradient	dP/dz	4.3	%/100m	Bolch (2007)
Temperature gradient	dT/dz	-0.51	°C/100m	Bolch (2007)
Threshold snow / rain	T_{thres}	1.5	°C	Calibrated (range -1-2.5°C)
Actual / potential evaporation	F_{ET}	70-100	%	Calibrated
Snowdrift onto glacier	SD_{gl}	2	-	Calibrated
Melt parameters				
Physical parameter	C_0	-50	W m^{-2}	Calibrated
Physical parameter	C_1	10	W m^{-2} K^{-1}	Oerlemans (2001)
Albedo Ice	α_{ice}	0.35	-	Calibrated (range 0.3-0.5)
Albedo Firn	α_{firn}	0.55	-	Calibrated (range 0.5-0.6)
Albedo Snow	α_{snow}	0.75	-	Calibrated (range 0.7-0.9)
Routing parameters				
Retention slow reservoir	r_{slow}	350	days	Calibrated
Retention ice & firn	r_{ice}	15	days	Calibrated
Retention snow	r_{snow}	20	days	Calibrated
Retention rock	r_{rock}	25	days	Calibrated
Retention pasture	$r_{low\_vegetation}$	40	days	Calibrated
Retention forest	r_{forest}	55	days	Calibrated

Climate parameters

Precipitation was interpolated along a gradient of +4.3% per 100 meters, which corresponds to 31 mm per 100 meters as calculated by Bolch (2007). This gradient is in the range of other studies in the region (Katchaganov, 2011; Hagg *et al.*, 2007). Precipitation was assumed to increase gradually until the crestlines (Katchaganov, 2011; Aizen *et al.*, 1995). This results in interpolated precipitation of 934 mm a^{-1} at 4000 m above sea level, which corresponds well with the results of Aizen et al. (2007; ~950 mm a^{-1}). A threshold of 1.5°C with a linear transition range of ±1°C has been applied to distinguish between solid and liquid precipitation (Ye *et al.*, 2013). Similar to Kuhn (2003), we redistributed a constant fraction of snow fall (SD_{gl} = 2) within the basin from ice-free areas to areas covered by glaciers, as wind and avalanches tend to erode snow from ridges and steep slopes and deposit it in valleys and cirques (Machguth *et al.*, 2006). This snowdrift leads to additional glacier accumulation and to reduced melting as a result of higher albedo for snow than ice.

Temperature was interpolated from Sabdan meteorological station using a gradient of -0.51% per 100 meters (Bolch 2007). This gradient is in the range of other studies in the region (Aizen *et al.*, 1995, 1996; Hagg *et al.*, 2013).

While potential evaporation can be much higher in arid Central Asia than in humid climates, actual evaporation is limited by the low water availability during dry summers (Hagg *et al.*, 2013). An empirical evaporation model is implemented in GERM, which calculates daily potential evaporation based on air temperature and the saturation vapor pressure (Huss *et al.*, 2008b; Hamon, 1961). The model considers five surface types (snow, ice, rock, low vegetation and forest) and has an interception reservoir. Potential evaporation is reduced to actual evaporation for each surface type using a factor F_{ET} that includes a function accounting for soil moisture. The parameters of the evaporation model are calibrated with the values given by Aizen et al. (2007) for the Chon Kemin valley. Modeled mean actual evaporation in the past (1955-1989) is 384 mm, which is in line with previous studies (Aizen *et al.*, 2007; Kuzmichenok, 2008).

Melt parameters

Two melt models are implemented in GERM: an enhanced temperature-index melt model (Hock, 1999; Huss *et al.*, 2008a) and a simplified energy balance equation for net surface energy flux (Oerlemans, 2001; Huss *et al.*, 2008b). The latter approach is less sensitive to temperature changes (Oerlemans, 2001; Pellicciotti *et al.*, 2005), which renders it particularly adequate for modeling in arid regions like Central Asia and over long time periods with significant temperature increases. In the energy balance equation below, the first parenthetical expression represents the shortwave radiation balance and the second parenthetical expression represents long-wave radiation balance and turbulent exchanges:

$$\psi = \{ a\,(1-\alpha)\,Q_E \} + \{ c_0 + c_1 T \}$$

- ψ daily mean surface energy flux (energy available for melting)
- a atmospheric transmission to solar irradiance (reduced incoming shortwave radiation due to cloudiness or haze)
- α surface albedo for snow, ice and firn
- Q_E clear-sky shortwave radiation (mean daily potential global radiation calculated from slope, aspect and topographic shading)
- c_0 parameter for turbulent heat exchange
- c_1 parameter for longwave radiation balance (10 W m^{-2}, Oerlemans 2001)

Parameter c_1 was set to 10 W m^{-2} K^{-1} and c_0 was used as a tuning parameter (Oerlemans, 2001; Machguth *et al.*, 2006; Painter *et al.*, 2013). Albedo had to be constrained for ice, firn and snow within the respective range of physical characteristics (Paterson, 1994).

Routing parameters

The water available for runoff is determined daily at every grid cell by solving the water balance using the calculated quantities for liquid precipitation, melt and evaporation (Huss *et al.*, 2008b). The runoff routing model is based on the concept of linear storage, with an interception-, slow- and fast reservoir (Farinotti *et al.*, 2012; Huss *et al.*, 2008b). Liquid precipitation first enters the interception reservoir. When the surface-type dependent capacity is exceeded, it is routed into the slow reservoir, which represents subsurface runoff components. The water volume added to the slow reservoir depends on the filling level and on the maximum capacity of the slow reservoir (Schaefli *et al.*, 2005). When the maximum capacity of the slow reservoir is reached, water is routed into the fast reservoir, which represents direct and near-surface runoff components. All reservoirs are emptied at a reservoir-dependent retention constant.

4.2 Calibration and validation results

Annual discharge is well reproduced by the model (Fig. S4). Monthly simulated and observed discharge reach a Nash-Sutcliffe model efficiency coefficient of E = 0.96 (Nash and Sutcliffe, 1970), as shown in Fig. S5.

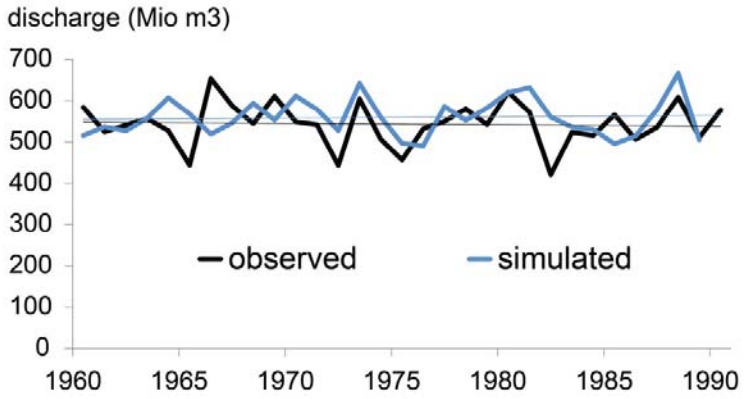

Fig. S4. Simulated and observed annual runoff at Karagai Bulak gauge (1959-1989).

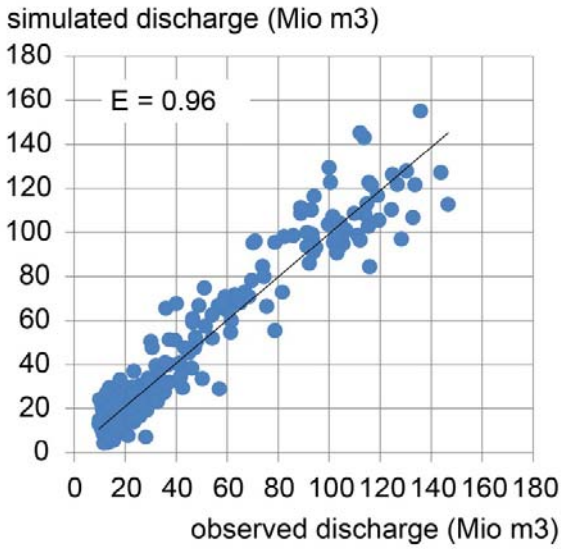

Fig. S5. Simulated and observed monthly runoff at Karagai Bulak gauge (1959-1989, with 1966-1977 excluded due to low quality of meteorological data).
The Nash-Sutcliffe model efficiency criterion E is 0.96 (Nash and Sutcliffe, 1970).

Simulated daily snow cover also corresponds well to visible snow cover on six selected Landsat scenes in 1977 and 1979 (Fig. S6); seasonal accumulation and melting of snow are thus reproduced realistically by the model. Simulated snow cover is displayed with a threshold of 15 mm snow water equivalents, which corresponds to 50 mm snow depth at a snow density of 300

kg m^{-3}. The accumulation season at Tuyuksu Glacier typically starts at the end of August or beginning of September (21/08-22/09) and stops in middle June (02/06-24/06), which is well reproduced by the model (Dyurgerov *et al.*, 1995; Aizen *et al.*, 1996; Schulz, 1965).

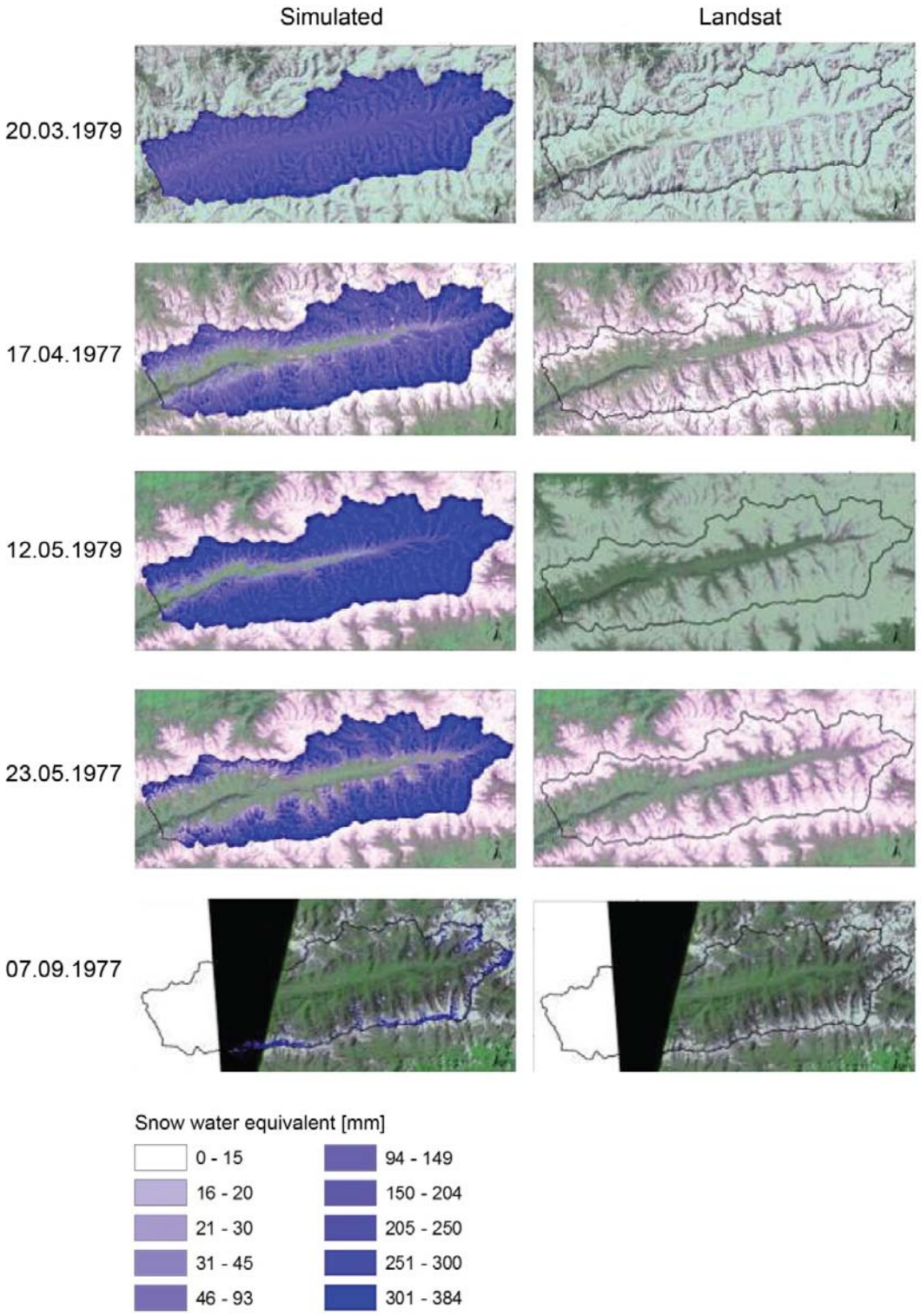

Fig. S6. Simulated and observed snow cover on six randomly chosen days in 1977 and 1979.

Annual snow cover duration is simulated within a 10% range of observed values from AVHRR satellite image analysis (Table S3); snow-rich and snow-poor years are thus well distinguished and the altitudinal snow distribution is well reproduced by the model. Days with more than 91 mm simulated snow water equivalents have been counted for snow cover duration. This higher threshold for AVHRR satellite images as compared to Landsat satellite images is due to the different resolution of AVHRR images (1 km) and Landsat images (30 m). Altitudinal patterns are well represented by the model and years with long snow cover duration (e.g. 1986) are well distinguished from years with shorter snow cover duration (e.g. 1987). Simulated mean annual snow cover duration was always in the range of the observed value ± 10%, except in 1989, when snow cover duration was slightly overestimated.

Table S3. Simulated and observed annual snow cover duration in the Chon Kemin valley (1985-1989).

	Snow cover duration [days]		
Year	**Observed mean**	**Observed ± 10%**	**Simulated mean**
1985	186	168-205	189
1986	218	196-240	206
1987	166	149-182	181
1988	181	163-199	181
1989	179	161-197	149

Simulated glacier surface mass balance and equilibrium line altitude (ELA) in the Chon Kemin valley show the same fluctuations at comparable levels as the series measured at Tuyuksu Glacier (Fig. S7). Simulated average ELA is 3875 m above sea level and thus corresponds to the previously assessed 3900 m above sea level in the Chon Kemin valley (Dyurgerov *et al.*, 1995). As a result of exposure to the North and the higher precipitation rate at Tuyuksu Glacier, ELA is slightly higher in the Chon Kemin valley than at Tuyuksu.

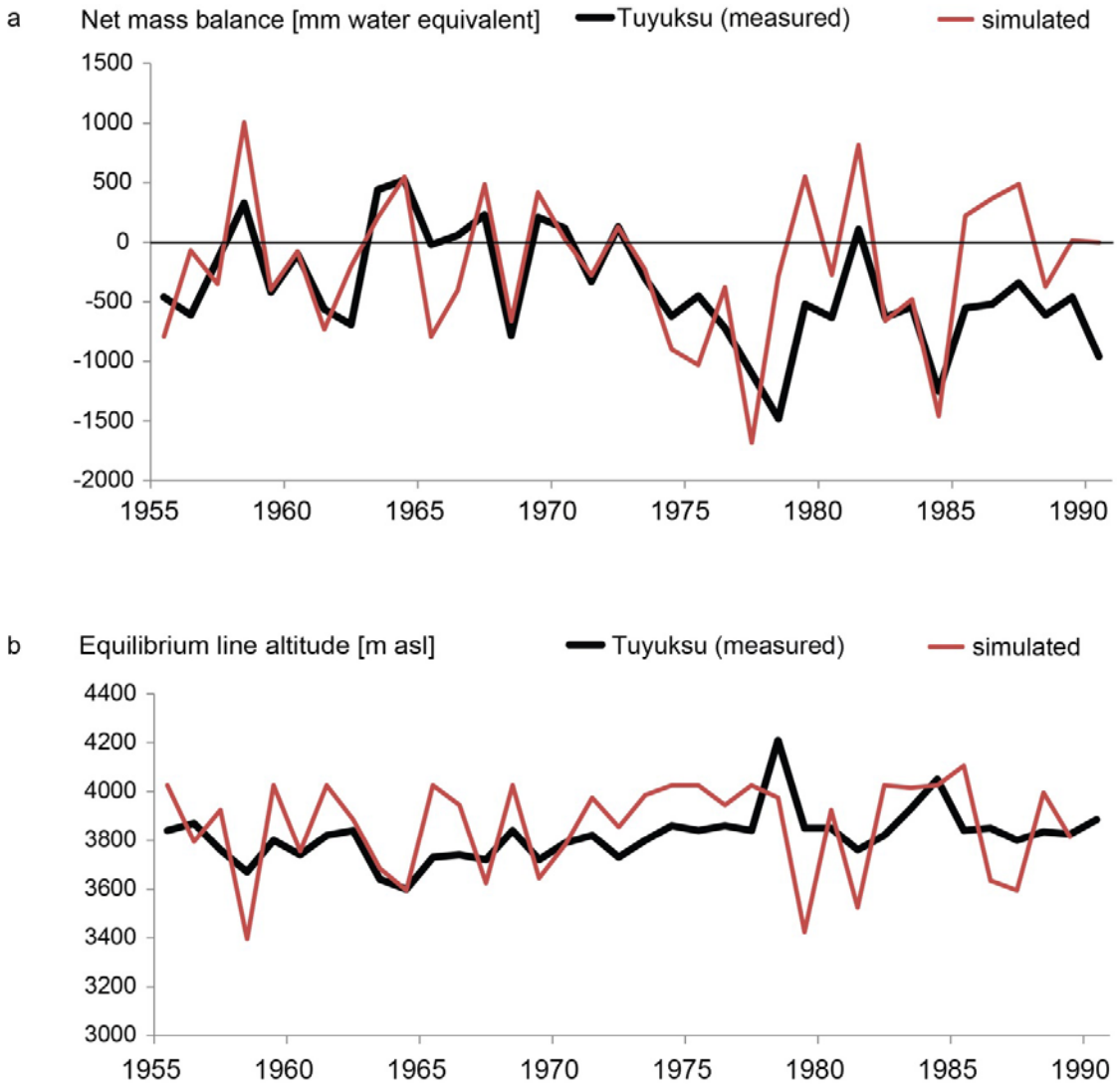

Fig. S7. Simulated and observed mass balance and equilibrium line altitude (ELA) between 1955 and 1990 in the Chon Kemin valley (simulated) and at Tuyuksu Glacier (measured).

The parameterization of glacier retreat is validated by comparing simulated with observed glacier shrinkage rates. The previously assessed annual shrinkage rate of 0.36% a^{-1} for the period 1955-1999 (Bolch, 2007) is reproduced exactly by the model.

References

Aizen V B, Aizen E M and Kuzmichenok V A 2007 Geo-informational simulation of possible changes in Central Asian water resources *Glob. Planet. Change* **56** 341-58

Aizen V B, Aizen E M and Melack J M 1995 Climate, snow cover, glaciers and runoff in the Tien Shan, Central Asia *Journal of the American Water Resources Association* **31** 1113-29

Aizen V B, Aizen E M and Melack J M 1996 Precipitation, melt and runoff in the northern Tien Shan *J Hydrol* **186** 229-51

Bolch T 2007 Climate change and glacier retreat in northern Tien Shan (Kazakhstan/Kyrgyzstan) using remote sensing data *Glob. Planet. Change* **56** 1-12

Dietz A, Kuenzer C, Conrad C and Dech S 2013 Changes of Snow Cover Characteristics in Central Asia between 1986 and 2012 derived from AVHRR and MODIS time series *Eastern Snow Conference*, Huntsville, Ontario, Canada

Dyurgerov M B, Liu C and Zichu X 1995 *Glaciers of Tien Shan (in Russian)* (Moscow: Publishing House VINITI)

Farinotti D, Usselmann S, Huss M, Bauder A and Funk M 2012 Runoff evolution in the Swiss Alps: projections for selected high-alpine catchments based on ENSEMBLES scenarios *Hydrol Process* **26** 1909-24

Fowler H J, Blenkinsop S and Tebaldi C 2007 Linking climate change modelling to impacts studies: recent advances in downscaling techniques for hydrological modelling *Int J Clim* **27** 1547-78

Hagg W, Braun L N, Kuhn M and Nesgaard T I 2007 Modelling of hydrological response to climate change in glacierized Central Asian catchments *J Hydrol* **332** 40-53

Hagg W, Hoelzle M, Wagner S, Mayr E and Klose Z 2013 Glacier and runoff changes in the Rukhk catchment, upper Amu-Darya basin until 2050 *Glob. Planet. Change* **110A** 62-73

Hamon W R 1961 Estimating potential evapotranspiration. *Journal of the Hydraulics Division-ASCE* **87** 107-20

Helsel D R and Hirsch R M 1992 *Statistical methods in water resources* (New York, USA: Elsevier)

Hock R 1999 A distributed temperature-index ice- and snowmelt model including potential direct solar radiation *J Glaciol* **45** 101-11

Huss M, Bauder A, Funk M and Hock R 2008a Determination of the seasonal mass balance of four Alpine glaciers since 1865 *J. Geophys. Res.* **113**

Huss M, Farinotti D, Bauder A and Funk M 2008b Modelling runoff from highly glacierized alpine drainage basins in a changing climate *Hydrol Process* **22** 3888-902

Immerzeel W W, Pellicciotti F and Bierkens M F P 2013 Rising river flows throughout the twenty-first century in two Himalayan glacierized watersheds *Nature Geosci* **6** 742-5

Jarvis J, H. , Reuter A N and Guevara E 2008 *Hole-filled SRTM for the globe, CGIAR-CSI SRTM 90 m Database, Version 4* (Montpellier, France: CGIAR Consort. for Spatial Inf)

Katchaganov S 2011 *Geomorphology and palegeography of the Chon Kemin basin in the Quaternary (in Russian)* (Bishkek: Institute of Geology, National Academy of Science of the Kyrgyz Republic)

Kendall M G 1975 *Rank correlation measures* (London: Charles Griffin)

Kirgizgidromet 1936-2002 *National Water Inventory* (Bishkek: Kirgizgidromet)

Kuhn M 2003 Redistribution of snow and glacier mass balance from a hydrometeorological model *J Hydrol* **282** 95-103

Kuzmichenok V A 2008 *Digital models of moisture characteristics in Kyrgyzstan (in Russian)* (Bishkek: Kyrgyz-Russian University)

Lutz A F, Immerzeel W W, Gobiet A, Pellicciotti F and Bierkens M F P 2013 Comparison of climate change signals in CMIP3 and CMIP5 multi-model ensembles and implications for Central Asian glaciers *Hydrol. Earth Syst. Sci.* **17** 3661-77

Machguth H, Paul F, Hoelzle M and Haeberli W 2006 Distributed glacier mass-balance modelling as an important component of modern multi-level glacier monitoring *Ann Glaciol* **43** 335-43

Meinshausen M, Smith S J, Calvin K, Daniel J S, Kainuma M L T, Lamarque J F, Matsumoto K, Montzka S A, Raper S C B, Riahi K, Thomson A, Velders G J M and Vuuren D P P 2011 The RCP greenhouse gas concentrations and their extensions from 1765 to 2300 *Clim Change* **109** 213-41

Nash J and Sutcliffe J 1970 River flow forecasting through conceptual models part I - A discussion of principles *J Hydrol* **10** 282-90

Oerlemans J 2001 *Glaciers and Climate Change* (Lisse: A.A. Balkema Publishers)

Painter T H, Flanner M G, Kaser G, Marzeion B, VanCuren R A and Abdalati W 2013 End of the Little Ice Age in the Alps forced by industrial black carbon *PNAS*

Paterson W S B 1994 *The physics of glaciers* (Oxford: Pergamon Press)

Pellicciotti F, Brock B J, Strasser U, Burlando P, Funk M and Corripio J 2005 An enhanced temperature-index glacier melt model including the shortwave radiation balance: development and testing for Haut Glacier d'Arolla, Switzerland. *J Glaciol* **51** 573-87

Prudhomme C, Reynard N and Crooks S 2002 Downscaling of global climate models for flood frequency analysis: where are we now? *Hydrol Process* **16** 1137-50

Schaefli B, Hingray B, Niggli M and Musy A 2005 A conceptual glaciohydrological model for high mountainous catchments *Hydrol. Earth Syst. Sci.* **9** 95-109

Schulz V L 1965 *Rivers of Central Asia (in Russian)* (Leningrad: Hydrometeoizdat)

Sen P K 1968 Estimates of the regression coefficient based on Kendall's tau *Journal of the American Statistical Association* **63** 1379-89

Smith J and Pitts G 1997 Regional climate change scenarios for vulnerability and adaptation assessments *Clim Change* **36** 3-21

Soviet Topographic Map 1988 *Chok-Tal, K-43-46 1:100'000* (Bishkek, Kyrgyzstan)

Taylor K E, Stouffer R J and Meehl G A 2012 An overview of CMIP5 and the experiment design *BAMS* **93** 485-98

Vuuren D, Edmonds J, Kainuma M, Riahi K, Thomson A, Hibbard K, Hurtt G, Kram T, Krey V, Lamarque J-F, Masui T, Meinshausen M, Nakicenovic N, Smith S and Rose S 2011 The representative concentration pathways: an overview *Clim Change* **109** 5-31

WGMS Haeberli W, Gärtner-Roer I, Hoelzle M, Paul F and Zemp M (ed) 2009 *Glacier Mass Balance Bulletin No. 10 (2006-07)* (Zurich: ICSU (WDS) / IUGG (IACS) / UNEP / UNESCO / WMO, World Glacier Monitoring Service) p 96

Ye H, Cohen J and Rawlins M 2013 Discrimination of solid from liquid precipitation over northern eurasia using surface atmospheric conditions *J Hydrometeorol* **14** 1345–55

Zhang X, Vincent L A, Hogg W D and Niitsoo A 2000 Temperature and precipitation trends in Canada during the 20th century *Atmosphere-Ocean* **38** 395-429